Available online at www.sciencedirect.com
ScienceDirect
Polymer 48 (2007) 3393–3399
polymer
www.elsevier.com/locate/polymer

Polymer Communication

'Butterfly' small-angle X-ray scattering patterns in semicrystalline polymers are double-elliptical

W. Wang [a], N.S. Murthy [b,*], D.T. Grubb [c]

[a] *Physics Department, University of Vermont, Burlington, VT 05405, United States*
[b] *New Jersey Center for Biomaterials, Rutgers University, 145 Bevier Road, Piscataway, NJ 088540, United States*
[c] *Department of Materials Science and Engineering, Cornell University, Ithaca, New York, 14853, United States*

Received 19 February 2007; received in revised form 11 April 2007; accepted 12 April 2007
Available online 19 April 2007

Abstract

We have previously shown that most small-angle scattering (SAS) patterns from a range of polymer fibers can be best fit using elliptical coordinates, where the minor axis of the ellipse is parallel to the fiber axis. Analysis of small-angle X-ray scattering patterns obtained during elongation of poly(ethylene-*co*-1-octene) films now shows that elliptical coordinates also provide a natural way to fit four-point radiating-out patterns, also called "butterfly" or "eyebrow" patterns. To fit this type of pattern the minor axis of the ellipse is tilted away from the fiber draw direction by some angle α, and as the films have rotational symmetry, the pattern is fitted with the sum of two ellipses, at $+\alpha$ and $-\alpha$. As a result, the reflections appear to fall on a hyperbolic arc – the butterfly pattern. The Matlab code to carry out this analysis on full 2D data is available on request. The elliptical analysis is primarily an empirical fit, much strengthened by its ability to be applied to all observed types of SAS patterns and by its relevance to the mechanical behavior of polymers.

Keywords: Elliptical small-angle scattering; Oriented polymer; Semicrystalline

1. Introduction

Discrete patterns that are seen in small-angle X-ray or neutron scattering (SAXS or SANS, SAS for either of them) of semicrystalline polymers fall into three categories: two-point bar shaped (Fig. 1a), four-point tilted inwards towards the equator (Fig. 1b), and four-point tilted outwards away from the equator (Fig. 1c, "butterfly" or "eyebrow patterns") [1]. Recently published data on poly(ethylene-*co*-1-octene) polymers, which show a remarkable range of drawing behaviors at different levels of octene, display all of these features [2,3]. Here we attempt to analyze these different types of patterns using a single scheme by describing the intensity distribution in these SAXS patterns in elliptical coordinates, and relate them to their mechanical properties.

Previously published data from 19 and 38 wt% 1-octene (Dow Chemical Company) referred to as low octene and high octene, respectively, will be used for this analysis [2,3]. Simultaneous SAXS and wide-angle X-ray diffraction (WAXD) data were obtained during deformation of 0.5 mm thick, 100 mm long and 15 mm wide films at HASYLAB, Hamburg, beamline A2 on an image plate with 1.5 Å wavelength radiation. Data were analyzed using codes written in Matlab.

2. Results

2.1. SAXS

The SAXS patterns are unoriented at zero strain. The two-point patterns that appear at ~100% elongation evolve into weakly resolved four-point patterns (Fig. 1a) at the maximum

* Corresponding author. Tel.: +1 732 445 0488x40020; fax: +1 732 445 5006.
E-mail address: murthy@biology.rutgers.edu (N.S. Murthy).

0032-3861/$ - see front matter © 2007 Elsevier Ltd. All rights reserved.
doi:10.1016/j.polymer.2007.04.026

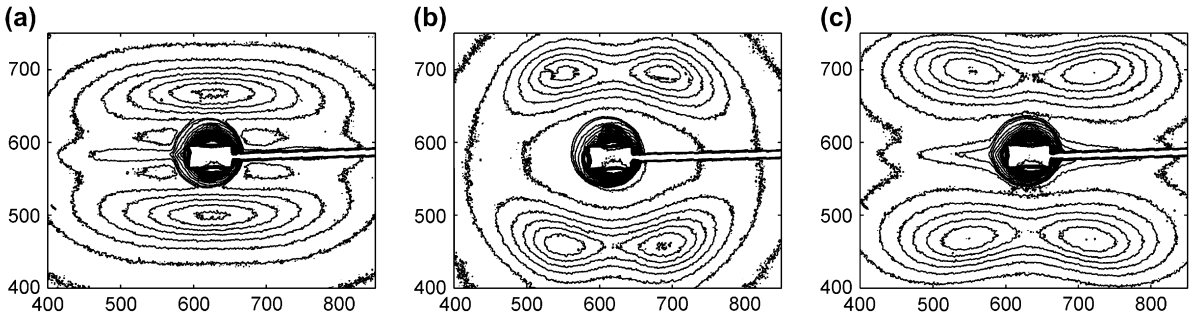

Fig. 1. Examples of the three types of SAXS patterns; fiber axis is vertical: (a) high-octene at 300% strain, two-point bar shaped (Fig. 7 in Ref. [2]); (b) high-octene relaxed to 190% strain after stretching to 600%, four-point tilted inwards (Fig. 7 in Ref. [2]); (c) low-octene relaxed to 360% strain after stretching to 500%, four-point and tilted outwards (Fig. 2 in Ref. [2]).

draw ratio (500% for low octene and 600% for high octene). When the stress is released these patterns transform into a four-point curved-in pattern in the high-octene polymer (Fig. 1b) and into a butterfly pattern in the low-octene sample (Fig. 1c) [3].

Fitting small-angle two- and four-point patterns from oriented polymers has empirically shown that most of them fall on a single ellipse [4–8]. This is illustrated in Fig. 2. Fig. 2a and c comes from the two-point pattern shown in Fig. 1a, and Fig. 2b and d from the four-point turned-in pattern shown in Fig. 1b. In (a) and (b) the positions Z_ϕ of peak intensity along Z-axis within the lamellar reflection are shown as circles and the line is the fitted ellipse. Figure (c) and (d) are the plots of $1/Z_\phi^2$ vs. $\tan^2\phi$ where ϕ is the azimuthal angle as shown on Fig. 2a. An ellipse follows Eq. (1), where $L_\phi = 1/Z_\phi$, and so gives a straight line on this plot [7]

$$L_\phi^2 = L_M^2 + L_E^2 \tan^2\phi \tag{1}$$

Here L_M and L_E are fitting constants. L_M is the periodicity in the lamellar stack oriented along the fiber axis, and is the commonly used lamellar spacing L. L_E is the (unobserved) lamellar

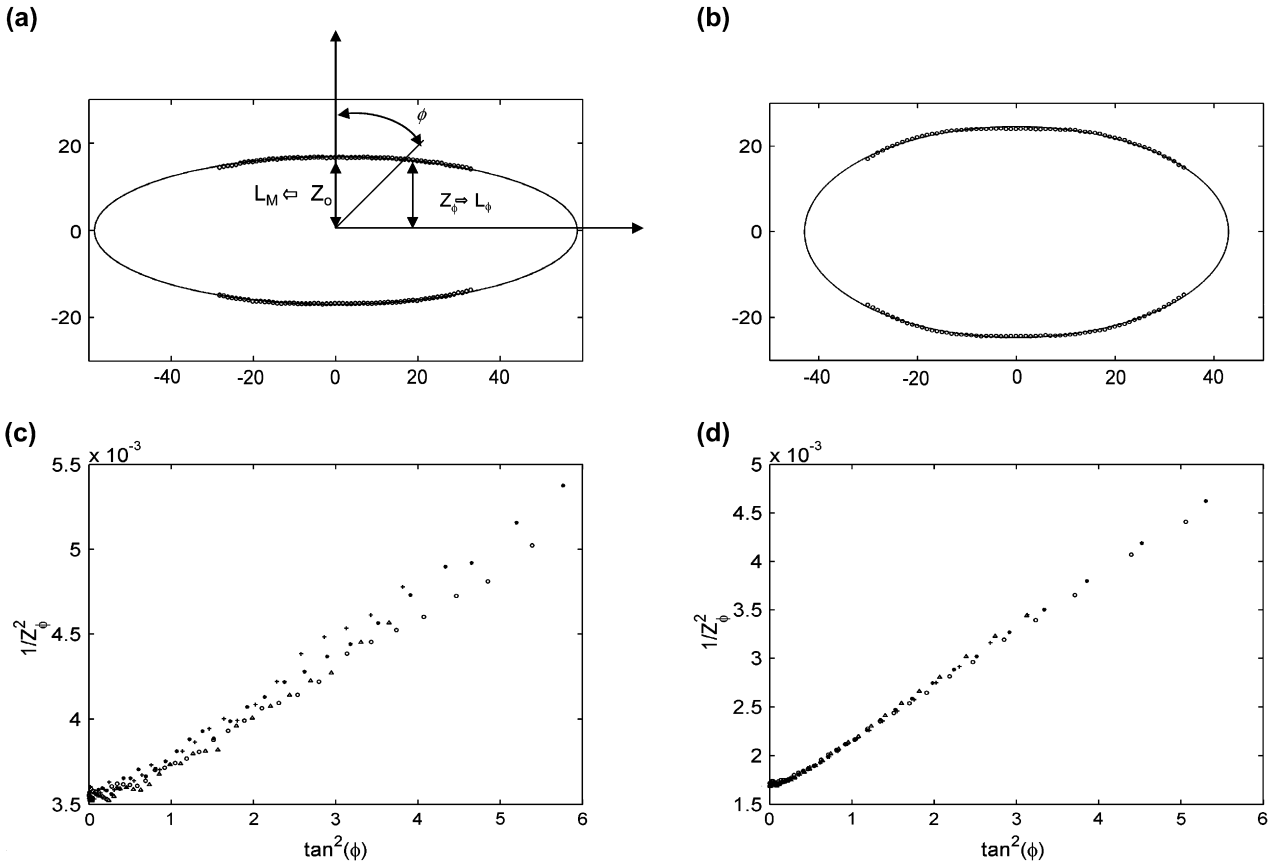

Fig. 2. Elliptical to patterns shown in Fig. 1. (a) and (c) refer to Fig. 1(a), and (b) and (d) refer to Fig. 1b. (a) and (b): the measured points are shown as circles and the fitted ellipse is overlaid on the observed data. (c) and (d): L_ϕ^2 ($1/Z_\phi^2$)–$\tan^2\phi$ plots of the lamellar peaks; data from the four quadrants are shown in four different symbols.

spacing in the equatorial direction. We have observed a straight line wherever there is enough intensity for a measurement, up to 78° in each quadrant [9].

To make this fit, the raw images were first rotated (in this instance by 1.5°) to make the symmetry axes horizontal and vertical. The images were then reduced into a 240 by 236 pixel image and divided into 236 slices parallel to the Z-axis. The intensity distribution along each slice was least-squares fitted to two Gaussian functions. Two values of Z corresponding to the lamellar peaks above and below the equator were obtained from each slice, and data from each quadrant are plotted with a different symbol in Fig. 2.

Fig. 3a and b are an attempt to use the same method to fit the butterfly SAXS pattern in Fig. 1c where the lamellar reflections appear to fall on hyperbolic arcs. Clearly it does not work well at all; data similar to this were observed in our earlier analysis of polyester fibers [9]. However, Fig. 3c and d shows that the data can be fitted extremely well by allowing there to be two tilted ellipses. One pair of reflections (in second and fourth quadrants) falls on one ellipse whose minor axis is rotated by an angle α away from the meridian, and another pair of reflections (in first and the third quadrants) on a second ellipse that is rotated by an angle $-\alpha$ (Fig. 3c). This second ellipse is automatically generated by the cylindrical symmetry of the sample.

Once the peak positions are obtained from the 2D image, either a one-ellipse or two-ellipse model is used to fit the trajectories of these positions. For the one-ellipse model (at low strains) these positions are assumed to fall on an ellipse defined by the major and minor axes, a and b, respectively, and the origin. A least-squares method, lsqcurvefit (Matlab), is used to obtain these fitting parameters. At strains of 300–600% where there was a ''dent'' along the minor axis and the trajectories look like a 'butterfly', we fitted the data to a two ellipse model. Again a least square method is used to obtain the five fitting parameters, a, b, α and the coordinates of the origin. This resulted in a linear $1/Z^2$ vs. $\tan^2\phi$ plot. The position of a point on the tilted ellipse is calculated in (X,Z) coordinates along the axes of the ellipse, then transformed to the original (X_o,Z_o) coordinates, see Fig. 4. For each point on the ellipse at an angle ϕ to the Z-axis, and a distance R from the origin we have:

$$\cot(\phi-\alpha)=\frac{Z_o}{X_o}$$

$$R^2=X^2+Z^2=X_o^2+Z_o^2 \qquad (2)$$

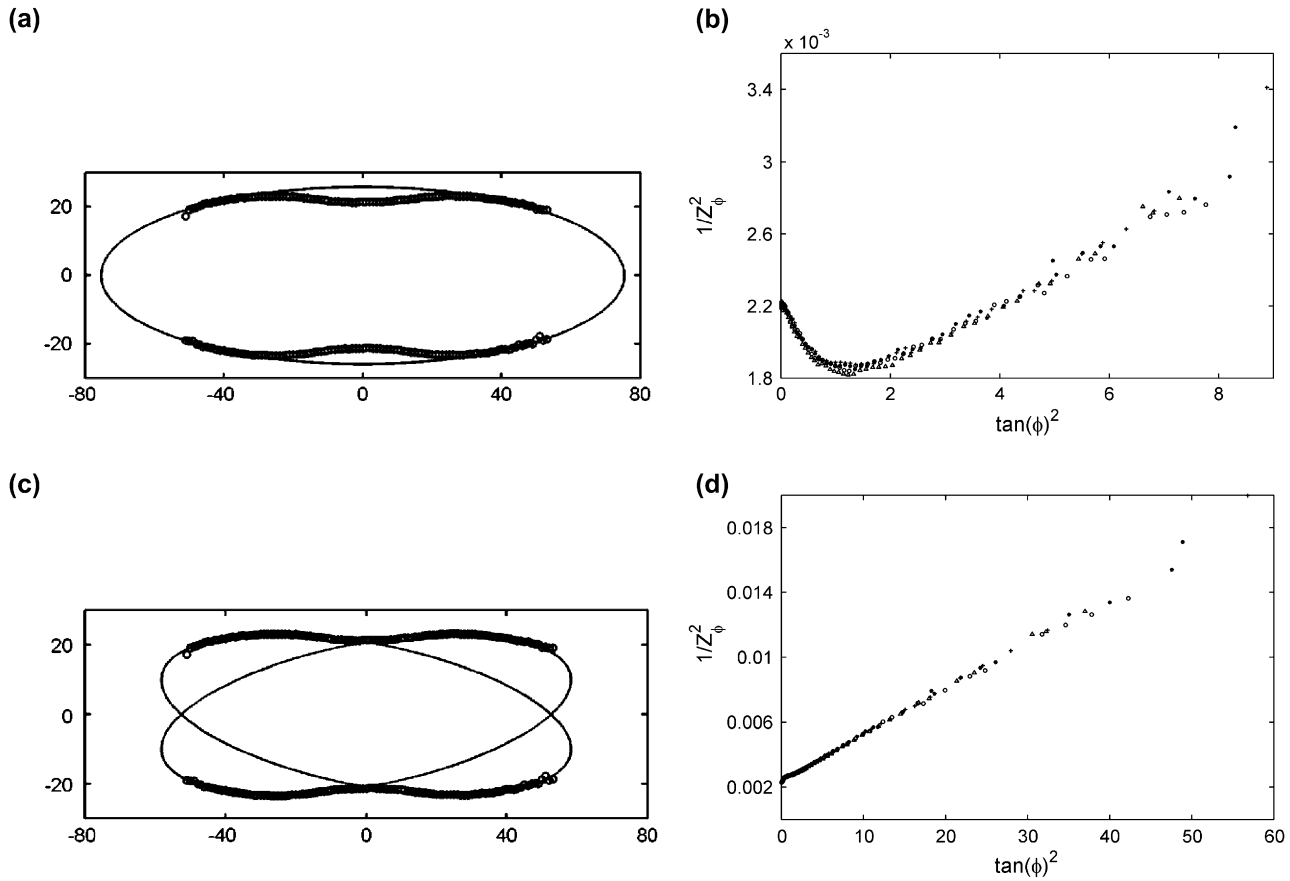

Fig. 3. Elliptical fits to the butterfly pattern shown in Fig. 1c. (a) Using one ellipse the X- and Z-coordinate of the maxima within the lamellar reflections measured at various azimuthal angles are shown as circles. (b) L_ϕ^2–$\tan^2\phi$ plots of the lamellar peaks in Fig. 1c. (c) Two-ellipse fit to the data in Fig. 1c (d) L_ϕ^2–$\tan^2\phi$ plots of the lamellar peaks interpreted as falling on two ellipses. The four regions are shown in four different symbols.

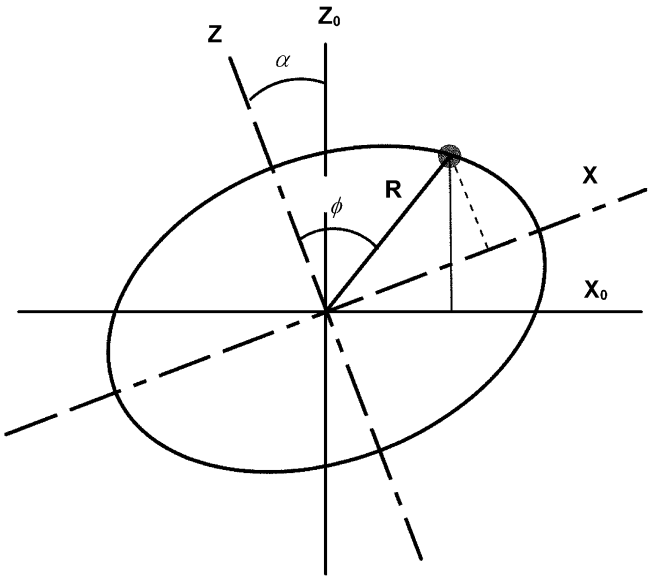

Fig. 4. Schematic of the coordinates used in fitting the tilted ellipse to the data.

ϕ (for a given α) and R are calculated from the measured (X_o,Z_o) values and since $Z_\phi = R\cos\phi = 1/L_\phi$ (in terms of fitting the tilted ellipse) a L_ϕ^2 vs. $\tan^2\phi$ plot can be created, as shown in Fig. 3d. The best fit value of α for Fig. 1c was 11°.

2.2. WAXD

WAXD orientation distribution was determined using the strong equatorial {110} reflection. At zero strain there is no orientation. Fig. 5a shows that at relatively low strains, there are two populations; one equatorial peak and one off-equatorial (giving two peaks by symmetry). Only the equatorial peak is present at high strains, Fig. 5b, and it remains the only peak when the stress is relaxed. This shows:

(i) that the structures giving rise to the tilted ellipse in SAXS have the chain direction of the crystallites aligned along the draw direction and
(ii) that the final structure is not the result of simple affine deformation of an initial isotropic structure, as intermediate states are more complex. The deformation causes crystallinity to rise while the initial structure is broken down and transformed into a new one [2,3].

Fig. 5c and d shows that the widths of the equatorial and off-equatorial peaks decrease with increasing strain. The orientation of the crystalline domains is partially reversible as can be seen in the decrease in the orientation in the films that were relaxed after taken to 500–600% strain. When the films relaxed, the crystalline orientation decreases to an intermediate value that is consistent with the residual macroscopic strain: the low-octene films have 150% residual strain and have a crystalline orientation close to that observed during stretching at 150% draw; the corresponding residual strain for high-octene film is 250%.

3. Discussion

A simple two-point SAXS pattern is normally considered as being due to a regular 1D repeating arrangement of crystals along a microfibril which is parallel to the draw direction. The microfibrils do not form a regular array, and positions of crystals in adjacent microfibrils are uncorrelated. A lateral spread of the two points into a bar pattern (Fig. 1a) is explained by having restricted lateral width of the diffracting element – a narrow microfibril with narrow crystals. In the lamellar model, strongly supported by microscopic views of highly crystalline polymers such as linear PE, the four-point pattern is interpreted as due to a tilt of the lamellar normal away from the draw direction as shown in Fig. 6a [6,10–15]. A lateral spread of these reflections, along a layer line, would then be explained by a limited width of the fibrils or stacks that lie along the fiber axis and contain these crystals with tilted surfaces.

The butterfly four-point pattern was observed in early studies of polyethylene sheets formed by rolling [10,15–17]. In these samples this pattern occurred when there was a splitting of the WAXD reflections, where the chain axis was no longer aligned along the extension direction. The spread of the spot was described, based on the analysis of insufficient data, as along a line at an angle α to the equator. By comparison with WAXD, this line was found to be perpendicular to a chain-axis direction as shown in Fig. 6b. By similar oversimplification of the SAXS data, Groves showed that with a combination of shear modes, it was possible to create all types of SAS patterns (with straight-line spreading) in systems with the chains aligned parallel to the draw direction [18]. In a model proposed by Gerasimov et al., reflection shape, which was derived from inadequate analysis of SAS patterns recorded on films, was accounted for by variation of a single parameter ($b\tan\phi/a$), where b is the width of the lamellae and a is the height of the lamellae [11]. The reflections spread along the layer line (bar pattern) for small values of $b\tan\phi/a$ (small tilt or narrow fibril) and along a radial line for large values of $b\tan\phi/a$. However, the spots in a butterfly pattern rarely extend radially.

A common feature of all of these models is that the spread of the reflections is due to a restricted width in some direction, and therefore the spread must be *along a straight line* in the same direction as this restricted width. That is, the models begin by setting the observed intensity (I) as:

$$I = |\overline{F}|^2 J$$

where F is the Fourier transform of the crystal shape, $|\overline{F}|^2$ is the cylindrically averaged shape factor of the mean crystallite (lamella) and J is the lattice factor or the interference function which depends only on the distribution of the centers of the crystallites. These models all derive from earlier work, when it was not possible to get quantitative analysis of the weak intensity tails of the reflections. The limited data can be fitted as a straight streak, allowing the use of a 1D lattice factor for J. No such simple interpretation is applicable when the spread is along a curved path, such as an ellipse. The data

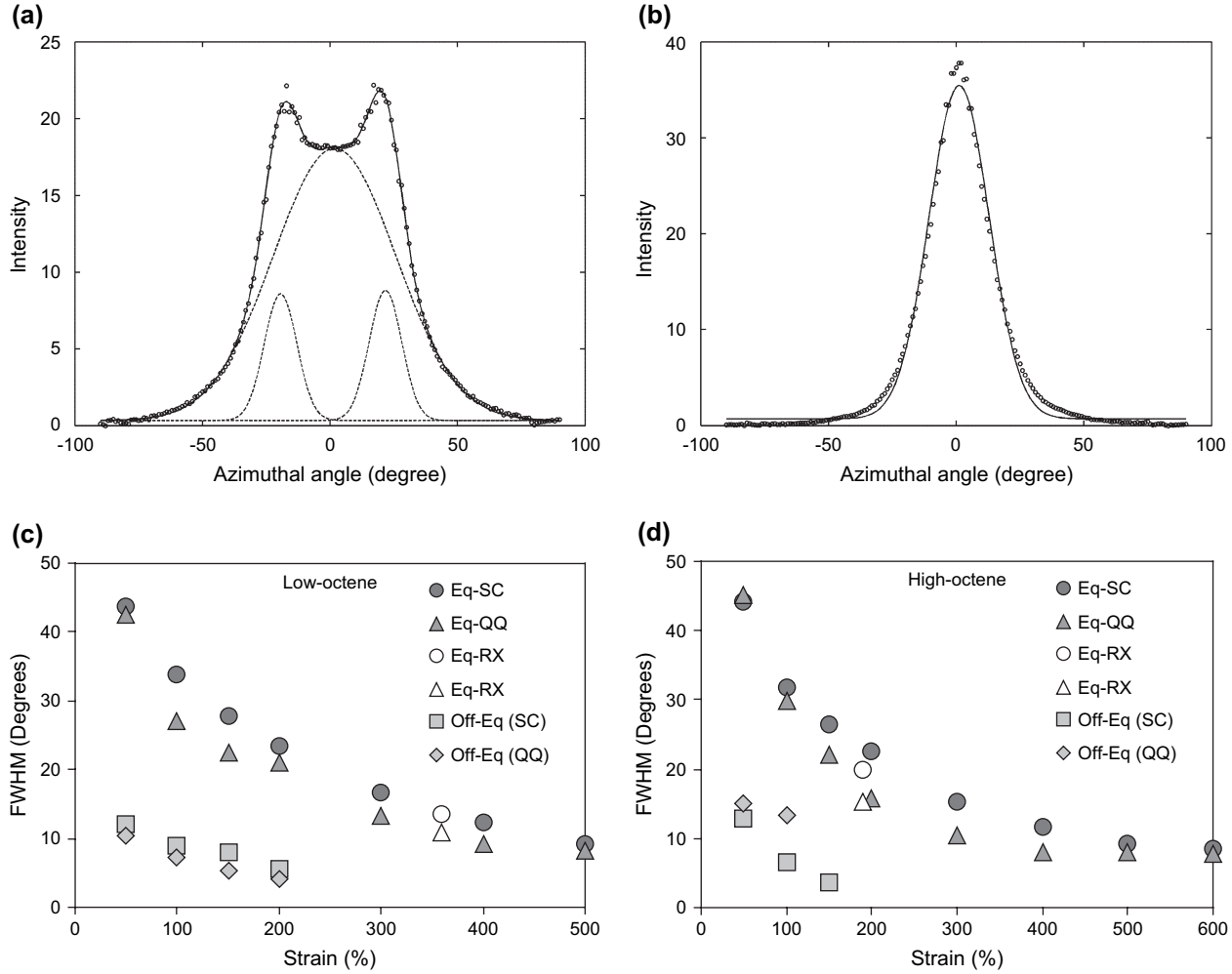

Fig. 5. Azimuthal distribution of intensity of {110} in low-octene films drawn to (a) 100% and (b) 300% strains. Full width at half-maximum (FWHM) of these peaks, which are inversely related to the degree of orientation, are plotted as a function of strain for (c) low-octene and (d) high-octene films. Eq and off-Eq refer to equatorial and off-equatorial peaks. SC and QQ refer to slow-cooled and quenched samples. Data marked RX are from relaxed samples.

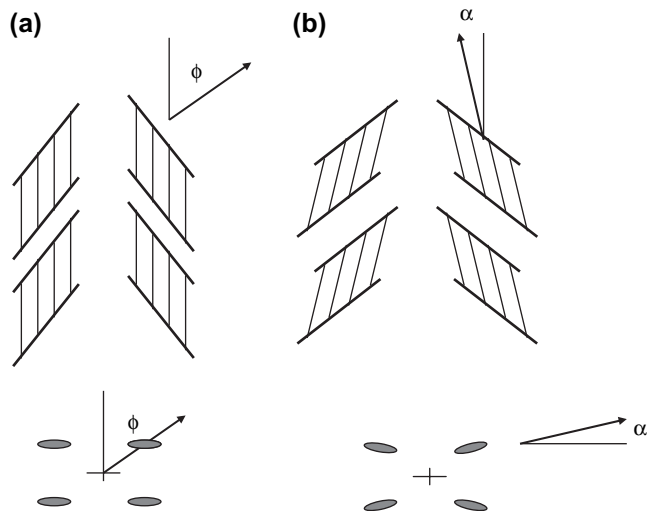

Fig. 6. Keller's model for four-point patterns [17]: (a) regular four-point pattern (the arrow is along the lamellae normal); (b) butterfly four-point pattern (the arrow is along the chain axis).

in Figs. 2 and 3 and in our earlier papers show clearly that when the whole reflection can be analyzed, it clearly does follow a curved track [4–8]. This curved track is often ignored even when analyzing data with good counting statistics [19]. However, it has been recognized that two angles are required to completely describe the SAS patterns, ϕ and α used here, ϕ and ψ in Ref [19], and ϕ and θ in Ref. [15].

One way to get a curved streak is by a range of misorientations of a 1D lattice. This spreads the intensity over spherical shells (resulting in Debye rings when the orientation is completely lost). The effect on the SAXS pattern is that intensity is spread along circular arcs. No combination of straight and circular spreadings is able to give the observed elliptical form. Another structural model was proposed by Zheng et al., who interpreted the spread of the SAXS reflection as due to paracrystalline disorder of a 3D macrolattice of lamellae. This cannot predict the observed curved streaks [20]. It was pointed out very early on that a lateral linear spread could be due to crystals with a range of tilts that had the same repeat distance in the fiber direction (and not due to a limited width) [16].

Clearly this can be generalized to crystals with a range of tilts and different repeat distances that create the observed curved streak. The lamellar spacings have to be correlated with the angle at which the diffraction appears [7,21]. It is not clear how this arises. The ellipse can thought of as describing the 3D correlation of lamellae centers of mass. In butterfly patterns the ellipse is tilted by some angle α away from the fiber axis. A single tilted ellipse can fit the data that are often seen in samples without cylindrical symmetry such as in some rolled and compression molded samples [16,17,21].

In earlier papers we proposed that an affine deformation of the lamellar lattice spreads the reflections along an ellipse [7,8]. This is an attractively simple idea: an isotropic lattice will give a circular reflection, and affine deformation of such a lattice will change the circle to an ellipse and concentrate the intensity towards the draw direction, as observed. This is true for instance in the case of a block copolymer. Here, the circular reflection is strong in the undrawn material, and the polycrystalline lattice can be seen in real-space (microscopic) studies [22]. On deformation of this system a continuous transformation with increasing ellipticity can be followed [23]. In contrast, in semicrystalline fibers there is no such continuous transformation, but often a complete breakdown of structure at a neck, with re-formation into structures with a new crystal spacing that depends on the drawing temperature. The change in structure in the films studied here can be followed clearly, but as shown in Fig. 5, the transformation is much more complicated than a simple affine deformation, so that explanation cannot be applied here. While affine deformation is a possible explanation of the elliptical forms, *it is not a universal one*.

Elliptical coordinates adequately account for the non-circular track in the currently available small-angle data. When data are empirically fit, there is always concern about the number of parameters involved. In the original fit using elliptical coordinates and a single ellipse, the small-angle pattern can be described using just three parameters [7,8]. These are the major and minor axes of the ellipse and the orientation ϕ of the peak intensity. The fits shown in Fig. 2a and b areas concerned only with the track of the peak, not the intensity profile, so these involve only two parameters. In the new version, the rotational angle of the ellipse, α, must be added to the list, so the fit in Fig. 3c uses three parameters, and the full fit of the pattern needs four. It is clear from the accurate fit to a large number of data points that the increase in parameters does not mean that the data are being fit arbitrarily. The simple models that give a straight-line spread of the reflection need three parameters in all cases. These are the lamellar spacing, the orientation ϕ of the peak intensity and the orientation of the direction of spread. The extra parameter is needed to give the ellipticity, which does not arise in the simple models.

Although we have focused here on fitting the track of the peak maxima to an ellipse, it should be noted that the entire SAXS intensity distribution can be fitted in elliptical coordinates by describing the intensity in terms of a suitable distribution (Gaussian/Lorentzian/Pearson VII function) centered around the peak maximum [8]. Such a fit provides a better fit with fewer parameters than those in Cartesian or polar coordinates, and may be used to extrapolate the data into the beam stop area or to the outskirts of the scattering where the measured data are noisy.

Characterizing SAS patterns as double or single elliptical is useful and relevant, as the different forms of the SAXS patterns relate to the mechanical behavior of the samples. The low-octene films that show a double-ellipse pattern when relaxed also exhibit strain hardening, while the high-octene films that show single-ellipse behavior when relaxed remain rubbery during elongation [3]. Further, while there is a large drop in long period L (from $\sim$250 Å to $\sim$150 Å) at low elongations (100%) in both polymers, L continues this decrease at higher elongations (500%) only in the rubbery high-octene films; it increases in the strain hardening low-octene polymers (Fig. 7). On the basis of SAXS and WAXD data [3], it appears that the long period seen at low elongations is due to micellar structures, and the decrease in L occurs when they transform

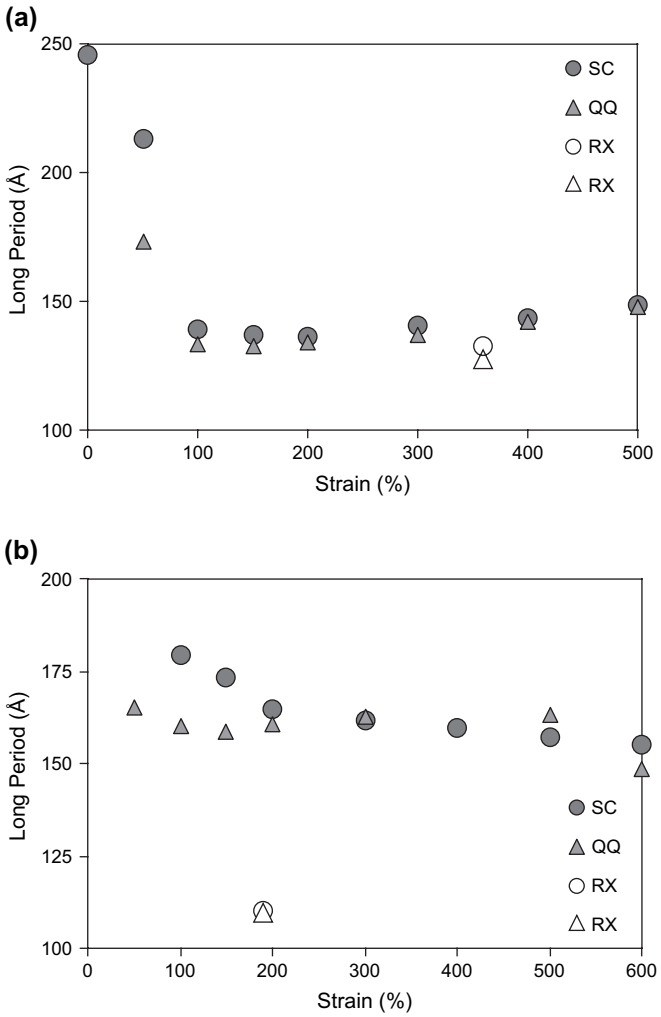

Fig. 7. Changes in the long spacing with strain: (a) low-octene PE; (b) high-octene PE. Circles and triangles are for slow-cooled (SC) and quenched (QQ) films, respectively. Open symbols correspond to relaxed samples (RX).

into lamellae. This transformation is complete in the low-octene films and the lamellar stacks reversibly stretch, increasing L, as they share the applied load on further elongation. The double ellipse in this polymer could be interpreted as due to 3D correlation of the movements of the lamellar centers of mass, e.g., progressive shear of the lamellae, as a result of interfibrillar and interlamellar tie molecules. On the other hand, in high-octene films, the lamellae continue to evolve even at 600% elongation, and L continues to decrease, reaching a much lower value (110 Å) when load is removed. The single ellipse in this polymer could be interpreted as due to random shear of still evolving lamellae due to the absence of ''crosslinks'' or correlations between them. In any case, there are significant mechanical differences and this can lead to different shear modes on relaxation that give rise to different patterns. It is worth noting that a stretched crosslinked network of strings have been implicated in butterfly patterns in small-angle light scattering (SALS) where it is sometimes called flattened butterfly or tulip pattern [24]. Similar diffraction patterns have also been seen from a lightly crosslinked aligned network of rods in a craze [25]. Our two-point pattern, referred to as a butterfly pattern in SALS literature, is attributed to axial correlations in density fluctuation and absence of such correlations in the equatorial direction [24,26].

4. Conclusions

Using data from drawn poly(ethylene-*co*-1-octene) polymers, it is found that all the observed types of small-angle patterns (two-point bar shaped, four-point tilted-in and tilted-out) can be analyzed by describing the intensity distribution in elliptical coordinates. Such analysis provides a few experimentally derivable parameters to characterize the lamellar structure. The tilt of the lamellae determines the movement of the lamellar reflections along the ellipse. Earlier analyses of the data from nylons and polyesters using similar methods have shown that these parameters greatly influence the performance of polymers. The analyses proposed here are applicable to any general nano-scale structure in which the crystalline domains are embedded in an amorphous matrix. Such analyses are useful for understanding the mechanical behavior of polymers and are applicable to similar patterns obtained from larger-length scale structures using SALS.

Acknowledgement

We thank Prof. N. Stribeck and his coworkers for generously providing us with the raw data that were used in this paper, and Profs. N. Stribeck and B. Crist for their constructive comments on the manuscript. This work was supported by NSF grant DMR-0513926.

References

[1] Balta-Calleja FJ, Vonk CJ. X-ray scattering of synthetic polymers. New York: Elsevier; 1989.
[2] Androsch R, Blackwell J, Chvalun SN, Wunderlich B. Macromolecules 1999;32:3735–40.
[3] Androsch R, Stribeck N, Lupke T, Funari SS. J Polym Sci Polym Phys 2002;40:1919–30.
[4] Murthy NS, Grubb DT. J Polym Sci Polym Phys 2002;40:691–705.
[5] Murthy NS, Grubb DT. J Polym Sci Polym Phys 2003;41:1538–53.
[6] Murthy NS, Grubb DT. J Polym Sci Polym Phys 2006;44:1277–86.
[7] Murthy NS, Grubb DT, Zero K. Macromolecules 2000;33:1012–21.
[8] Murthy NS, Zero K, Grubb DT. Polymer 1997;38:1021–8.
[9] Murthy NS, Grubb DT, Zero K, Nelson CJ, Chen G. J Appl Polym Sci 1998;70:2527–38.
[10] Cowking A, Rider JG, Hay IL, Keller A. J Mater Sci 1968;3:646–54.
[11] Gerasimov VI, Genin YV, Kitaigorodsky AI, Tsvankin DY. Kolloid Z Z Polym 1972;250:518–29.
[12] Gilman TH, Resetarits MR, Crist JB. Polym Eng Sci 1978;18:477–87.
[13] Ginzburg BM, Sultanov N. J Macromol Sci Phys 2001;B40:207–30.
[14] Young RJ, Bowden PB, Ritchie JM, Rider JG. J Mater Sci 1973;8:23–36.
[15] Hay IL, Keller A. J Mater Sci 1967;2:538–58.
[16] Point JJ, Homes GA, Gezovich D, Keller A. J Mater Sci 1969;4:908–18.
[17] Pope DP, Keller A. J Polym Sci Polym Phys 1975;13:533–66.
[18] Groves GW, Hirsch PB. J Mater Sci 1969;4:929–32.
[19] Chen X, Burger C, Fang D, Sics I, Wang X, He W, et al. Macromolecules 2006;39:5427–37.
[20] Zheng Z, Nojima S, Yamane T, Ashida T. Macromolecules 1989;22:4362–7.
[21] Song HH, Argon AS, Cohen RE. Macromolecules 1990;23:870–6.
[22] Sakamoto N, Hashimoto T. Macromolecules 1998;31(24):8493–502.
[23] Brandt M, Ruland W. Acta Polym 1996;47:498–506.
[24] Kadoma IA, Egmond JWv. Langmuir 1997;13:4551–61.
[25] Yang AC-M, Kramer EJ. J Mater Sci 1986;21:3601–10.
[26] Milner ST. Phys Rev 1993;48(5):3674–91.